ELSEVIER

Tectonophysics 339 (2001) 443–454

TECTONOPHYSICS

www.elsevier.com/locate/tecto

Receiver function structure beneath three southern Africa seismic broadband stations

V. Midzi[a,*], L. Ottemöller[b]

[a]*Department of Meteorological Services, Goetz Observatory, P. O. Box AC65, Ascot, Bulawayo, Zimbabwe*
[b]*Institute of Solid Earth Physics, University of Bergen, Alleg. 41, N-5007 Bergen, Norway*

Received 3 February 2000; accepted 11 May 2001

Abstract

The shear wave velocity structure beneath three southern African stations, Lusaka (LSZ), Lobatse (LBTB) and Boshof (BOSA) were estimated using the time domain inversion of stacked teleseismic receiver functions. Broadband teleseismic 3-component waveform data were used in a source equalisation procedure to estimate radial and transverse receiver functions for each station. The radial receiver functions were stacked according to the following criteria, an azimuthal interval of ±15°, similar ray parameter and shape. For the shield-based stations BOSA and LBTB simpler receiver functions than for LSZ, which is located in the Irumide belt, were obtained. The lateral variation in receiver functions with azimuth as observed at each station stems from lateral heterogeneities beneath each station. The velocity models were presented as P wave velocity models. From these models, the crust mantle transition zones beneath LSZ and BOSA were determined at depths of about 37–44 km and 34–38 km respectively. For LBTB, the northeast quadrant velocity model displayed a clear mantle-continent transition zone in the depth range 40–45 km, whilst the Moho depth in the southern quadrants is not as clear. Beneath all the stations, we observed a low velocity zone, which appears to correlate with the cratonic velocity structure. This feature is consistent with crustal structure results obtained in other cratonic or shield-based crustal studies. The results in this study contribute crustal structure information, which has been lacking at BOSA, LBTB and LSZ.

Keywords: crust; receiver function; shear velocity; Southern Africa; teleseismic events

1. Introduction

The receiver function method is a powerful tool employed in the investigation of the earth's shear velocity structure. By inverting receiver functions, it is possible to constrain the Moho depth and the average shear wave velocity beneath a recording station (Owens et al., 1987; Langston, 1989; Ammon, 1991; Ammon and Zandt, 1993; Mangino et al., 1993; Gurrola et al., 1994; Kaspar and Ritter, 1998; Sandvol et al., 1998). Though southern Africa is an interesting region with respect to tectonic evolution, so far there is limited detailed information on the crustal structure. The majority of crustal structure studies, have been performed on the Kaapvaal craton (Fig. 1), South Africa.

These studies employed seismic reflection and refraction methods (Willmore et al., 1952; Gane et al., 1956; Hales and Sacks, 1959; Durrheim and Green, 1992). Stuart and Zengeni (1987) investigated the structure of the Limpopo mobile belt and southern Zimbabwe craton using seismic refraction. Van Zijl

* Corresponding author. Tel.: +263-9-66197; fax: +263-9-77811.

E-mail address: vunganai@hotmail.com (V. Midzi).

0040-1951/01/$ - see front matter
PII: S0040-1951(01)00124-X

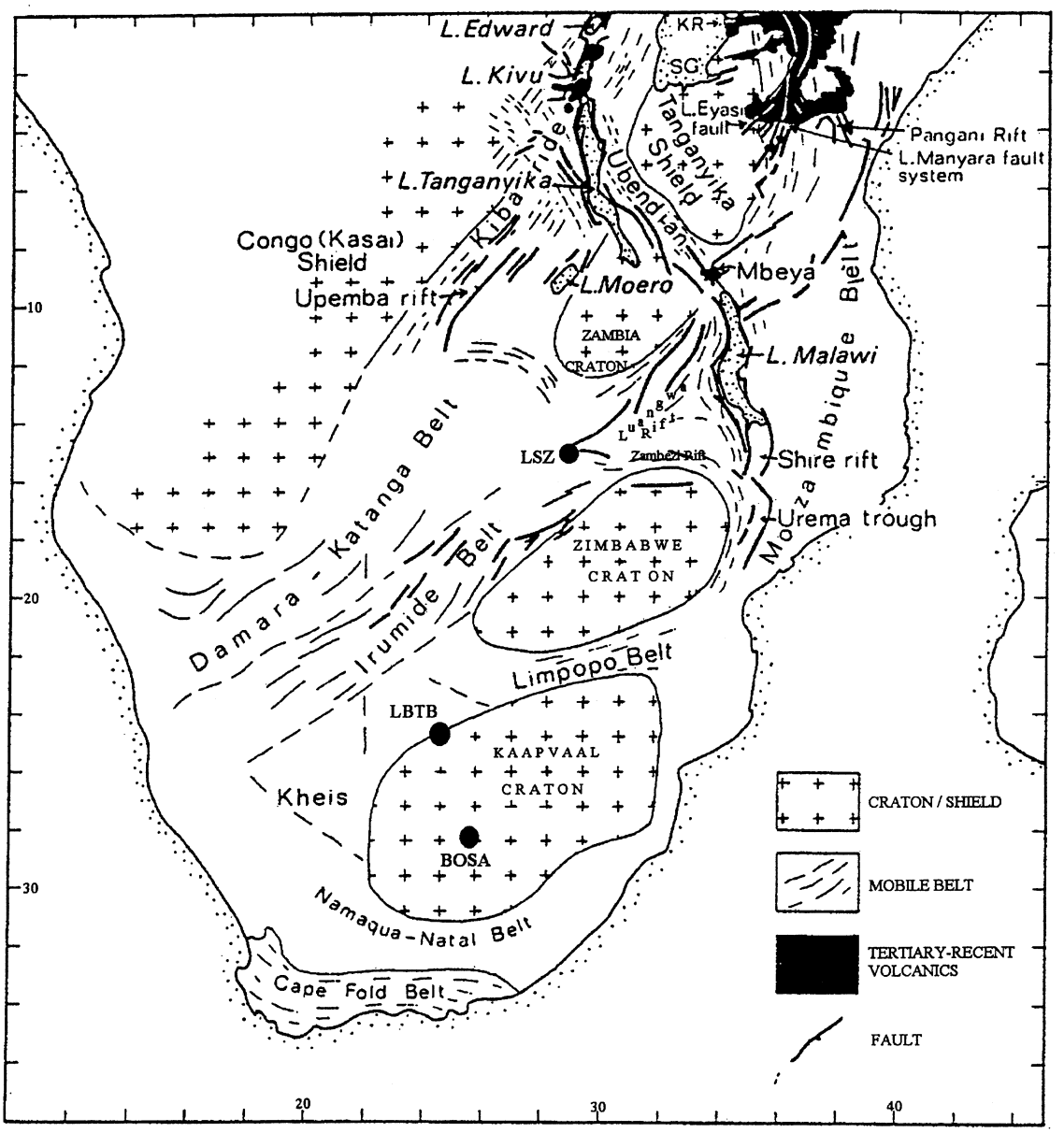

Fig. 1. Map showing the general geology of southern Africa (adapted from Fairhead and Stuart, 1982) and the location of the three digital broad-band seismic stations BOSA, LBTB and LSZ (black dots).

(1978) used an electrical resistivity profile to investigate the crustal structure of the same region. Bloch et al. (1969) employed surface wave group and phase velocities to estimate an average velocity structure beneath southern Africa. Qiu et al. (1996) used several different seismic methods to study the same region including receiver functions. However, their purpose was not to produce definitive models of the velocity structure beneath the stations and thus only obtained a gross structure. For example only one receiver function was used for the Lusaka station. Therefore, not much emphasis was placed on the results from this

Table 1
The locations of the southern African digital stations used in this study

Code	Site name	Latitude	Longitude	Elevation
LSZ	Lusaka, Zambia	−15.2766	28.1882	1184.8
LBTB	Lobatse, Botswana	−25.0145	25.5970	1128.0
BOSA	Boshof, South Africa	−28.6131	25.4156	1280.0

part of their study. Nevertheless, their results are the only published crustal thickness values beneath the stations, Lusaka (LSZ, 42 km), Lobatse (LBTB, 44 km), and Boshof (BOSA, 35 km). Wright and Hall (1990) used seismic profiling to estimate cratonic, mobile belts and sedimentary basin Moho depths in the Nosop basin in Botswana. In their global and continental studies Nakanishi and Anderson (1984); Hadiouche and Jobert (1988) used surface wave group and phase velocities to investigate the sub-crustal velocity structure beneath southern Africa.

Other studies include heat flow observations (Chapman and Pollack 1977; Ballard and Pollack, 1987; Nyblade et al., 1990) and gravity measurements (Brown and Girdler, 1980; Gwavava et al., 1992, 1996) over the region.

Due to the deployment of IRIS broadband stations in southern Africa valuable data for use in crustal structure studies have become available. The aim of this study is to investigate the shear wave velocity structure beneath the southern African stations, BOSA, LBTB and LSZ. The location of the stations in the region is shown in Fig. 1 and Table 1. This figure also shows the tectonic units of the region, which is dominated by cratonic units welded together by Proterozoic mobile belts (Qiu et al., 1996). The geologic and tectonic evolution of this region is discussed thoroughly in earlier publications (Kroner, 1977; Stuart and Zengeni, 1987;de Wit et al., 1992; Gwavava et al., 1992, 1996). BOSA is located on the southwestern part and LBTB on the northwestern part of the Kaapvaal craton, whilst LSZ is located north of the Zimbabwe craton in the Irumide mobile belt (Fig. 1, Table 1).

2. Receiver function

The receiver function is a time series, sensitive to velocity changes in the crust beneath a seismic station. It is obtained through the deconvolution of the vertical component from the horizontal components. The resulting waveform comprises of P-to-S converted phases, whose amplitudes and timing can be modelled to provide constraints on the Moho depth and underlying shear wave velocity structure. Langston (1979); Ammon et al. (1990); Cassidy (1992) presented the method in earlier studies.

In this paper we shall only discuss two important parameters associated with the method. These are the water-level constant and the Gaussian width, a. In the frequency domain deconvolution, the receiver function $H(w)$ is obtained by deconvolving the vertical component $Z(w)$ of an earthquake recording, from the radial component $R(w)$; i.e.

$$H(w) = \frac{R(w)Z^*(w)}{\phi(w)}G(w) \tag{1}$$

where:

$$\phi(w) = \max\{Z(w)Z^*(w), c\max\{Z(w)Z^*(w)\}\} \tag{2}$$

$Z^*(w)$ is the complex conjugate and c is the water-level constant. The water-level constant limits the value of the denominator in Eq. (1) (Clayton and Wiggins, 1976; Mangino et al., 1993), to avoid dividing by zero. We used a value of 0.001.

The Gaussian filter is represented by:

$$G(w) = \exp\left\{\frac{-w^2}{4a^2}\right\} \tag{3}$$

where a is the Gaussian width factor. High values of a were found to give noisy receiver functions. The level of scattering in such receiver functions would be enough to lead to potentially biased inversion results (Mangino et al., 1993), whereas this potential is greatly reduced at long periods.

The receiver function from a smaller value of the Gaussian width tends to smooth over the effects of small-scale crustal heterogeneities and produce

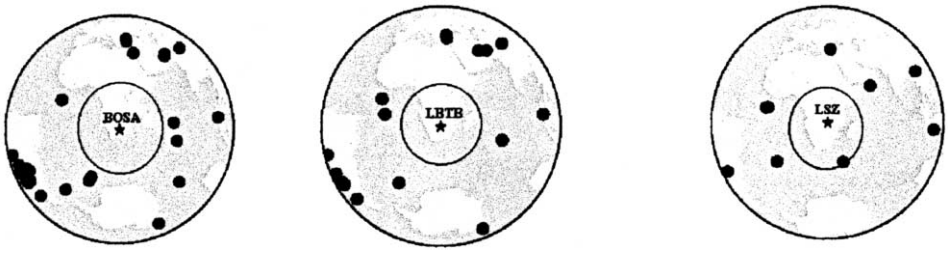

Fig. 2. Maps showing location of events whose records were used in calculating the receiver functions. The inner circle marks a distance of 30° from the station, whilst the outer circle marks 90°.

simpler structures with layer thickness resolutions equal to or greater than 7 km. We report the results obtained using a Gaussian width factor of 1.5.

3. Data

The three stations, BOSA, LBTB and LSZ have been operated as digital broadband stations since February 1993, April 1993 and August 1994, respectively. Data are transferred to the IRIS Data Management Centre (DMC). We obtained 87, 72 and 35 teleseismic earthquake records from the DMC that were recorded at BOSA, LBTB and LSZ respectively. The operation of the stations has been rather unstable, reducing the number of suitable events, especially for LSZ.

Before deconvolution the data were processed by windowing the direct P phase, rotating to the theoretical back-azimuth of the event and picking the arrival time. Noisy records were discarded and the remainder deconvolved to calculate the radial and tangential receiver functions. Fig. 2 shows maps of the events from which the final receiver functions were calculated.

As in most receiver function studies, (Owens, 1984; Ammon and Zandt, 1993; Mangino et al., 1993), the receiver functions were stacked according to ray parameter and back-azimuth values in order to reduces the noise due to scattering.

Compared to LSZ, the stations BOSA and LBTB have simple receiver functions (Fig. 3). This might be expected since BOSA and LBTB lie on the more homogeneous Kaapvaal craton, whereas LSZ is situated in the Irumide mobile belt. Low velocity sedimentary rocks overlying high velocity crystalline rocks usually result in large amplitude phases 2–3 s after the direct P phase. This is observed on some of the receiver functions from all three stations, but more so for LSZ. The azimuthal distribution of the receiver functions at all the stations is not good enough to resolve the possible dip of layers.

3.1. Lusaka (LSZ)

Fig. 4A illustrates the stacked receiver functions for LSZ from three quadrants, northeast, southeast and southwest. The receiver functions are different from each other, implying a significant variation in crustal structure with azimuth. Within the first 5–7 s after the direct P phase, we observed two P-to-s converted phases. In all cases the first Ps phase has large amplitudes, very likely representing a large velocity change between low velocity sedimentary rocks and high velocity crystalline rock. After these phases, the northeast receiver function (Baz = 48) is more complex, with several significant phases.

On the southeast quadrant receiver function (Baz = 158), the only other significant phase, after the P-to-s converted phases, is the multiple phase, which arrives 20 s after the direct P phase.

There are two stacked receiver functions shown for the southwest quadrant, at back azimuth (baz) 235 and 241°. These are actually within the azimuth criteria of 15° used in the stacking. However, the source depths and epicentral distances of the earthquake events are different, i.e. 10 km depth, epicentral distance of 67° and 500 km depth, epicentral distance of 88°, for baz = 235 and 241° respectively. These differences imply that the incident angle of the baz-235° receiver function is greater than that of baz-241°. Consequently, the Ps phases sample areas of different

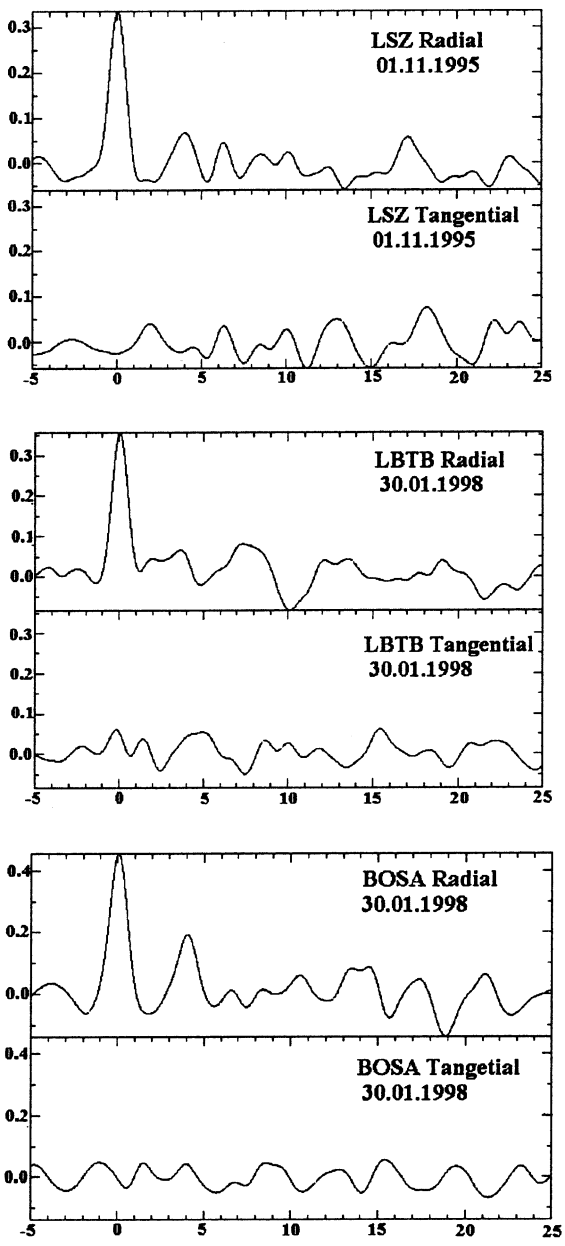

Fig. 3. Examples of 'good' radial and tangential receiver functions selected for the inversion for velocity structure beneath each station.

sizes, with the baz-235 receiver function sampling a larger area. The Ps phase on the baz-241 receiver function arrives 1 s ahead of the baz-235 receiver function. This should translate to different Moho depths. The cause is likely due to the difference in

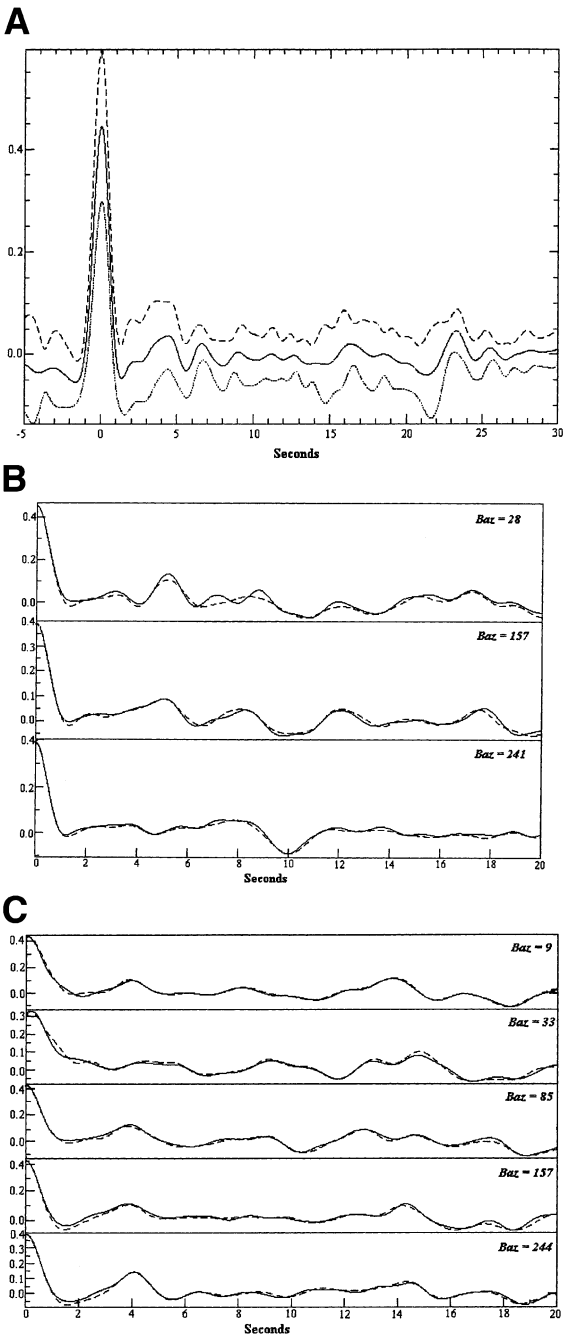

Fig. 4. (A) The solid line represents the stack of all the observed receiver functions and the broken lines are the limits for all receiver functions at LSZ. (B) Observed (broken line) and synthetic (solid line) receiver functions for LBTB. (C) Observed (broken line) and synthetic (solid line) receiver functions for BOSA.

the sampling areas, with the baz-235 receiver function probably sampling thicker crust further south.

3.2. Lobatse (LBTB)

The stacked receiver functions for LBTB are shown in Fig. 4B. These represent the earth response to seismic waves arriving from the northeast (Baz = 28), southeast (Baz = 157) and southwest (Baz = 241) quadrants beneath LBTB. Of these, the southwest quadrant receiver function is the least complicated. The most distinct phase apart from the direct phase is the multiple phase appearing 10 s after the direct P phase. The timing and size of the multiple phase amplitude implies a strong velocity contrast at a depth between 15 and 20 km below the surface. Two weak Ps phases are observed in the first 5 s after the direct P phase and a third after 6 s that is probably due to the Moho discontinuity. The northeast receiver function is more complex. The dominant phases are the strong Ps phase, 5 s after the direct P phase, and two multiple phases 12 and 14 s after the P onset. Beside these major phases, there are several smaller phases, which testify to the complex nature of the velocity structure beneath the station.

Several strong phases are observed in the southeast quadrant receiver function. A Ps phase occurs 5 s after the direct P phase. A strong multiple phase is also observed at 10 s, again implying a strong velocity discontinuity at a depth between 15 and 20 km below the earth surface.

The differences among the receiver functions from the three quadrants reflect a laterally complex earth structure beneath LBTB. A feature that is persisting in all the receiver functions is the multiple phase occurring 10 s after the direct P phase. Considering its time of arrival, there must be a strong discontinuity or velocity contrast at a depth between 15 and 20 km.

3.3. Boshof, BOSA

Though BOSA had more data than the other two stations, we could also only obtain good-stacked receiver functions for three quadrants, northeast, southeast and southwest with the northeast quadrant sampled by stacks of three receiver functions. Fig. 4C shows the observed stacked receiver functions at BOSA. Immediately, one observes the strong Ps conversion phase 4 s after the direct P phase, on all the receiver functions. This implies a clear Moho discontinuity beneath the station. The northeast quadrant receiver functions are more complex compared to the rest but similar to each other. Within 20 s after the direct P phase, four strong phases are observed on the three receiver functions in the northeast quadrant, the P-to-s converted and three multiple phases.

The southeast quadrant is represented by a single stack of receiver functions. A surface low velocity layer can explain the strong negative pulse, which immediately comes after the direct P phase. This is followed by a P-to-s converted phase. The next strong phase is a multiple phase at 15 s after the direct P phase, followed by a negative polarity pulse representing a multiple phase (Owens et al., 1987; Ammon et al., 1990; Ammon, 1991).

The southwest quadrant receiver function is very similar to that in the southeast. It also has a strong negative pulse immediately after the direct P phase, followed by the P-to-s converted and the multiple phases. This similarity in the receiver functions should correlate with a structure, which does not change much from southwest to southeast beneath BOSA and only slightly more complicated in the northeast. The Moho depth should be similar in the three quadrants, considering the onset time of the P-to-s converted phase. The larger amplitude of the southwest quadrant receiver function Ps phase could mean a sharper Moho discontinuity.

4. Inversion results

The receiver functions are inverted using a time domain waveform inversion scheme. The method is based on the inversion method of Owens (1984). It is an implementation of a more efficient algorithm for calculating differential seismograms (Randall 1989) and the ‘jumping’ inversion technique of Shaw and Orcutt (1985). A more thorough explanation of this method can be found in Ammon et al. (1990). The receiver function is sensitive to shear wave velocity. However, we presented the results as P velocity models by assuming a Poisson ratio of 0.25, to facilitate easier comparison with results from other studies.

An important assumption of the time domain inversion technique is that the initial model is close to the

true earth velocity structure (Ammon et al., 1990). Thus a priori data are important in determining the initial model used in the inversion. The initial models used for BOSA and LBTB were derived from earlier structure studies on the Kaapvaal craton. Since no structure studies have been reported for the area at or around LSZ, we used results from studies in the Limpopo mobile belt to construct the initial model. For BOSA and LBTB stations, a gross solution of the structure was obtained by inverting a receiver function obtained by stacking all the receiver functions. We further refined the initial model by synthetic forward modelling.

However, a limited number of good quality receiver functions were observed to be in a position to be stacked in different azimuths for LSZ. As a result we only inverted the receiver function obtained by stacking all the ten observed receiver functions using four different initial models.

A factor considered in the inversion is the trade-off between model roughness and rms (Ammon, 1991). Large roughness values lead to good fits, but very rough and unrealistic solutions. A smoothness factor of $\sigma = 0.1$ was observed to give realistic solutions, and also gave the same rms fit between synthetic and observed receiver function as for the pre-signal noise.

4.1. LSZ

The velocity models in Fig. 5A show the final inversion models for the three quadrants northeast, southeast and southwest around LSZ. In all cases, inversions of the receiver functions produced good fits to the observations (Fig. 5A).

It should be noted that in the following discussion the Moho is sometimes referred to as the crust-mantle boundary especially where there is a transition zone.

Assuming the Moho occurs at P wave velocity of about 7.8 km/s, the crust-mantle boundary in the northeast quadrant is relatively sharp and has a transition zone of approximately 40–43 km below the surface. The crustal structure above the Moho has two clear sections of different average velocities. The upper section, which is referred to as the upper crust, has an average velocity of about 6 km/s and a lower boundary at 22 km beneath the surface. The lower section or lower crust has an average velocity of 7 km/s and is located between 22 and 40–43 km beneath the surface. The two P-to-s converted phases observed on the stacked receiver function must be due to the crust-mantle boundary and lower-upper crust boundary.

The southeast quadrant model shows a structure that is quite different from that of the northeast quadrant. The main differences are the low velocity surface layer and the low velocity zone centred at a depth of 19 km beneath the surface. The upper boundary of the low velocity zone must have generated the P-to-s converted phase that is observed 3 s after the direct P phase on the receiver function (Fig. 5a). The mid-crust low velocity zone is consistent with results obtained elsewhere and in other southern Africa seismic studies (Bloch et al., 1969; Fuchs and Landisman, 1966; Mueller and Landisman, 1966; Gutenberg, 1955) on crustal structure. This phenomenon has mostly been observed beneath cratons. Therefore, this must imply that the receiver function in the southeast quadrant also samples part of the Zimbabwe craton.

Beneath 20 km the velocity increases gradually with depth to about 34 km where it increases sharply. Thereafter, the velocity is constant for about 7 km before another sharp increase. This second sharp increase is very likely the crust-mantle boundary, since the P wave velocity increases from 7 to about 7.9 km/s at this stage.

The inversion of receiver functions in the southwest quadrant produced models that are different from those obtained in the northeast and southeast quadrants. This quadrant has two models whose receiver functions have different slowness values. One model (slowness 0.071 s/km) shows a crust with an average velocity of about 6.6 km/s to a depth of 40 km. Between 40 and 45 km, the velocity increases gradually to about 7.9 km/s. This marks a crust-mantle transition of about 5 km thick. It displays high velocity sub-surface layers in the depth range, 2–8 km. The second model (slowness 0.042 s/km) has a high velocity layer between 2 and 8 km with velocities greater than 7 km/s. Such a high value of the velocity is not realistic at this depth and can be a manifestation of the inversion process. However, it is conceivable that there is a high velocity layer at these depths considering that the general geology of this area consists of white and red sandstones overlain by basaltic lavas (Maufe, 1924;

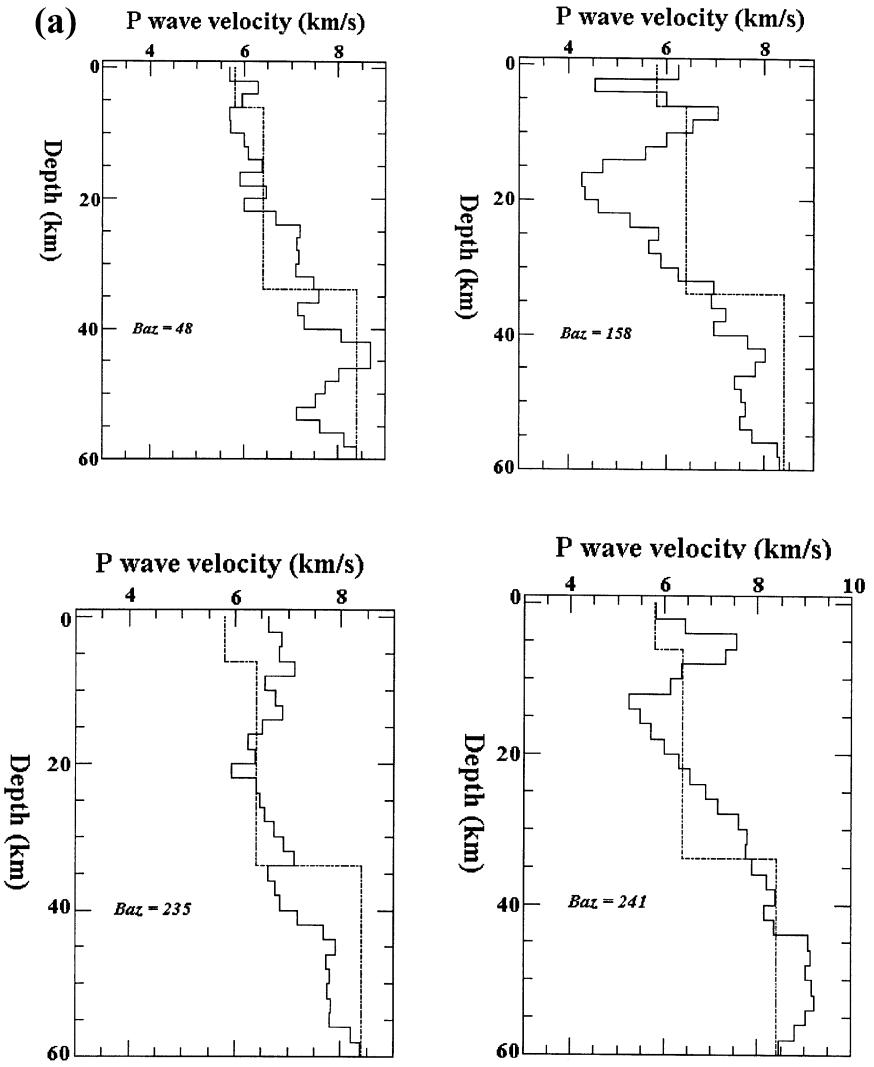

Fig. 5. (A) Inversion results for LSZ. (i) Solid line is the average velocity model and the broken lines represent the standard deviation, (ii) observed (solid line) and synthetic (broken lines) receiver functions from the four starting models. (B) Inversion results for LBTB and BOSA. The solid line model is the average of models from northeast, southeast and southwest quadrants. The broken line models are the standard deviation.

Vail, 1967; Reeves and Hutchings, 1975). Below the high velocity layer the velocity increases to 7.5 km/s at a depth of 30 km. It further increases between 30 and 37 km to 8 km/s, where it remains constant up to 44 km. Since the Moho is assumed to occur at 7.8 km/s, the crust-mantle boundary here occurs between 37 and 44 km beneath the surface.

4.2. LBTB

We inverted three stacked receiver functions from the northeast, southeast and southwest quadrants. The results are shown in Fig. 5B. The final models were not very different from each other; therefore, we calculated an average velocity model and the standard

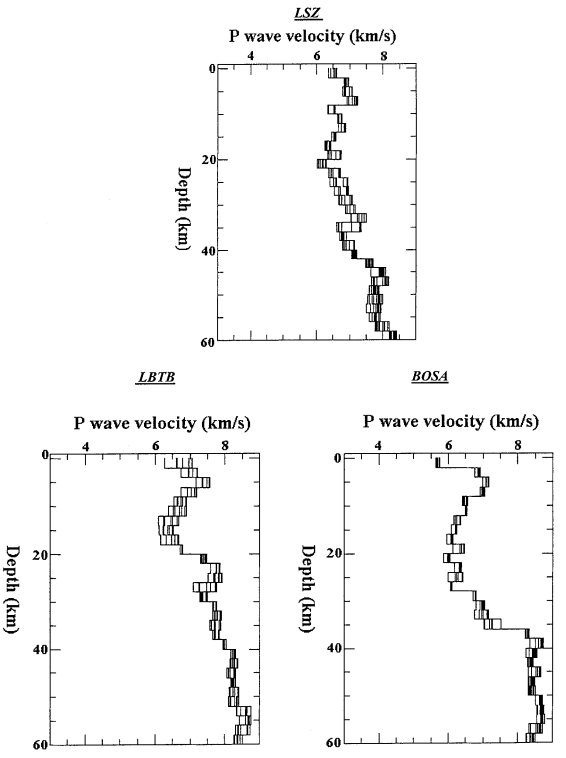

Fig. 6. Twelve acceptable velocity models resulting from 120 waveform inversions of the southwest radial receiver function at each of the stations, LSZ, LBTB and BOSA. Each model produces a synthetic waveform that compares well to the observed receiver functions

deviations. The models differ mostly in the upper mantle, where there is a velocity change of 0.8 km/s. An upper crust low velocity zone about 15 km thick overlies a lower crust of average velocity of about 7 km/s. A crust—mantle transition zone of about 7 km is observed from a depth of approximately 37 km.

4.3. BOSA

As with the two sites discussed above, we obtained velocity models for the northeast, southeast and southwest quadrants beneath BOSA. The models were similar and an average velocity model with the standard deviations was plotted (Fig. 5B). The difference of 0.8 km/s observed between the standard deviations points to significant lateral velocity differences beneath BOSA. The crust-mantle boundary depth is constrained very well in all quadrants and is shown between 34 and 38 km.

5. Discussion

The crustal structure results described above are actually the first seismic results that have been published for the three stations. Vinnik et al. (1996), used receiver functions to estimate velocity structure beneath BOSA and LBTB among other stations. However, they were more interested in much deeper structure. Reflection and/or refraction studies in the western part of the Kaapvaal craton obtained Moho depths of about 36 km (Willmore et al., 1952), 35 km in the centre of the craton (Gane et al., 1956; Durrheim and Green, 1992) and 37 km in the east (Hales and Sacks, 1959). These compare well to values of 34–38 km obtained at BOSA, which is located in the southern part of the craton. LBTB is located in the northwestern part of the craton and the Moho transition zone is between 40 and 45 km. These compare well to results obtained by Wright and Hall (1990) in reflection and refraction studies near LBTB. The results obtained for LSZ provide the first such models for the area.

The non-uniqueness in the inversion of receiver functions was discussed by Ammon et al. (1990). We investigated this aspect and the initial model dependency. This was accomplished by perturbing an initial model by a maximum cubic perturbation of 0.5 km/s and a maximum random perturbation of 0.1. The results for all three stations are shown in Fig. 6.

All synthetic receiver functions calculated from these models fitted the observed receiver functions well. At each station the models are not very different from each other. A slightly larger range in velocities, 0.5, is observed in the upper crust beneath LBTB. However, the ranges of the models at all the stations are small enough to represent them by one model.

The ability of the receiver functions to resolve the shear wave velocity change at a boundary depends on the noise level in the receiver functions. For records with low noise (e.g. ~0.04 P_z, Cassidy, 1992), it has been shown that the minimum velocity change (ΔV_s) that can significantly affect the P-to-s converted phase's amplitude lies between 0.2 and 0.4 km/s

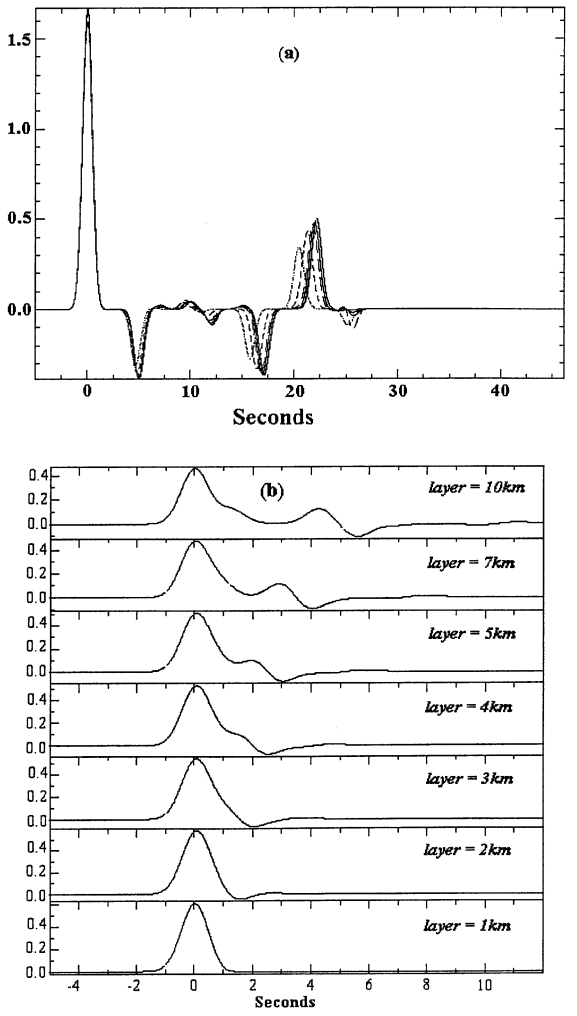

Fig. 7. Plots of receiver functions from a forward modelling procedure to investigate the minimum shear wave velocity that can receiver produce a change on the function (a) and the minimum resolvable layer thickness (b).

(Cassidy, 1992). Since the receiver functions used in this study had low frequency content, we assume a minimum velocity change of about 0.4 km/s. To confirm this we performed forward modelling and the results are shown in Fig. 7. We also used forward modelling to determine the minimum layer thickness (ΔZ) that can be resolved by low frequency receiver functions (i.e. Gaussian factor = 1.5). The results in Fig. 7 show that our data can resolve layers of at least 7 km thickness. The ΔV_s and ΔZ values can also be used as the error levels in the final velocity models.

6. Conclusion

We estimated the crustal structure beneath LSZ, LBTB and BOSA by inverting stacks of teleseismic receiver functions. The resulting velocity models are presented as P wave velocity models. We presented all the models for LSZ individually because the velocity differences between them are more pronounced. In the northeast quadrant two clear discontinuities were observed in the crust, the Conrad discontinuity observed at a depth of 22 km and a sharp crust-mantle transition zone at 40–43 km. The main features in the crustal structure model in the southeast quadrant are surface and mid-crust (19 km) low velocity layers. The Moho is observed at a depth of about 41 km. The southwest quadrant models are characterised by sub-surface high velocity layers that are likely a reflection of the high velocity sandstone and basaltic rocks in the area. The crust–mantle boundary is in the depth range, 37–44 km. Of the three stations the crust information obtained for LSZ is the most important since no previous seismic crustal structure information for it has been published.

Though some other earlier geophysical studies have been carried out near BOSA and LBTB, the results from this study are the first for these stations. The crust-mantle boundary beneath BOSA is sharply defined in all quadrants and on average the boundary is observed between 34 and 38 km. The crust mantle transition zone beneath LBTB is found at depths between 37 and 45 km. We also observed pronounced upper crust low velocity zones beneath LBTB and the southern quadrants models for LSZ.

Acknowledgements

The authors are grateful to Juan Pablo Ligorría, Department de Estudios y Desarrollo Geotérmico, Guatemala, for the valuable advice during the processing of our data. The excellent guide by Chuck Ammon on receiver functions proved very helpful during the study.

References

Ammon, C.J., 1991. The isolation of receiver effects from

teleseismic P wave fronts. Bull. Seismol. Soc. Am. 81, 2504–2510.

Ammon, C.J., Randall, G.E., Zandt, G., 1990. On the nonuniqueness of receiver function inversions. J. Geophys. Res. 95, 15303–15318.

Ammon, C.J., Zandt, G., 1993. Receiver structure beneath the southern Mojave block, California. Bull. Seismol. Soc. Am. 83, 737–755.

Ballard, S., Pollack, H.N., 1987. Diversion of heat by Archaean cratons: a model for southern Africa. Earth and Planetary Letters 85, 253–264.

Bloch, S., Hales, A.L., Landisman, M., 1969. Velocities in the crust and upper mantle of southern Africa from multi-mode surface wave dispersion. Bull. Seismol. Soc. Am. 59, 1599–1629.

Brown, C., Girdler, R.W., 1980. Interpretation of African gravity and its implication for the break-up of the continent. J. Geophys. Res 85 (B11), 6443–6455.

Cassidy, J.F., 1992. Numerical experiments in broadband receiver function analysis. Bull. Seismol. Soc. Am. 82, 1453–1474.

Chapman, D.S., Pollack, H.N., 1977. Heat flow and heat production in Zambia: Evidence for lithospheric thinning in central Africa. Tectonophysics 41, 79–100.

Clayton, R.W., Wiggins, R.A., 1976. Source shape estimation and deconvolution of teleseismic body waves. Geophys. J. R. Astron. Soc. 47, 151–177.

de Wit, M.J., Roering, C., Hart, R.J., Armstrong, R.A., de Ronde, C.E.J., Green, R.W.E., Tredoux, M., Peberdy, E., Hart, R.A., 1992. Formation of an Archaean continent. Nature 357, 553–562.

Durrheim, R.J., Green, R.W.E., 1992. A seismic refraction investigation of the Archaean Kaapvaal Craton, South Africa, using mine tremors as the energy source. Geophys. J. Int. 108, 812–832.

Fairhead, J.D., Stuart, G.W., 1982. The seismicity of the East African rift system and comparison with other continental rifts. In: Palmason, G. (Ed.), Continental and Oceanic Rifts. Geodyn. Ser. Am. Geophys. Union, 5; pp. 41–61.

Fuchs, K., Landisman, M., 1966. Detailed crustal investigation along a north–south section through the central part of western Germany. Geophys. Monogr. 10, 433–452.

Gane, P.G., Atkins, A.R., Sellschop, J.P.F., Seligman, P., 1956. Crustal structure in the Transvaal. Bull. Seism. Soc. Am. 46, 293–316.

Gurrola, H., Minster, J.B., Owens, T., 1994. The use of velocity spectrum for stacking receiver functions and imaging upper mantle discontinuities. Geophys. J. Int. 117, 427–440.

Gutenberg, B., 1955. Wave velocities in the Earth's crust. In: Poldervaart, A. (Ed.), The Crust of the Earth, Geophysical Society of America, Special paper 62, pp. 19–34.

Gwavava, O., Swain, C.J., Podmore, F., Fairhead, J.D., 1992. Evidence of crustal thinning beneath the Limpopo belt and Lebombo monocline of southern Africa based on regional gravity studies and implications for the reconstruction of Gondwana. Tectonophysics 212, 1–20.

Gwavava, O., Swain, C.J., Podmore, F., 1996. Mechanics of isostatic compensation of the Zimbabwe and Kaapvaal cratons, the Limpopo Belt and the Mozambique basin. Geophys. J. Int. 127, 635–650.

Hadiouche, O., Jobert, N., 1988. Geographical distribution of surface–wave velocities and 3-D upper-mantle structure in Africa. Geophys. J. 95, 87–109.

Hales, A.L., Sacks, I.S., 1959. Evidence for an intermediate layer from crustal structure studies in the eastern Transvaal. Geophys. J. R. Astron. Soc. 2, 15–33.

Kaspar, T., Ritter, J.R.R., 1998. P-SV conversions of teleseismic waves beneath Chyulu hills volcanic field, Kenya. Geophys. Res. Let. 25, 559–562.

Kroner, A., 1977. Precambrian mobile belts of southern and eastern Africa: Ancient sutures or sites of ensialic mobility? A case for crustal evolution towards plate tectonics. Tectonophysics 40, 101–135.

Langston, C.A., 1979. Structure under Mount Rainier, Washington, inferred from teleseismic body waves. J. Geophys. Res. 84, 4749–4762.

Langston, C.A., 1989. Scattering of teleseismic body waves under Pasadena, California. J. Geophys. Res. 94, 1935–1951.

Mangino, S.G., Zandt, G., Ammon, C.J., 1993. The receiver structure beneath Mina, Nevada. Bull. Seismol. Soc. Am. 83, 542–560.

Maufe, D.H., 1924. An outline of the geology of southern Rhodesia. S. Rhod. Geol. Surv., short report No.17.

Mueller, S., Landisman, M., 1966. Seismic studies of the earth's crust in continents. 1. Evidence for a low-velocity zone in the upper part of the lithosphere. Geophys. J. R. Astron. Soc. 10, 525–538.

Nakanishi, I., Anderson, D.L., 1984. Measurements of mantle wave velocities and inversion for lateral heterogeneity and anisotropy. 2. Analysis by the single-station method. Geophys. J. R. Astron. Soc. 78 (2), 573–617.

Nyblade, A.A., Pollack, H.N., Jones, D.L., Podmore, F., Mushayandebvu, M., 1990. Terrestrial heat flow in east and southern Africa. J. Geophys. Res. 95, 17371–17384.

Owens, T.J., 1984. Determination of crustal and upper mantle structure from analysis of broadband teleseismic P-waveforms. PhD thesis, Department of Geology and Geophysics, The University of Utah.

Owens, T.J., Taylor, S.R., Zandt, G., 1987. Crustal structure at regional seismic test network stations determined from inversion of broadband teleseismic P waveforms. Bull. Seismol. Soc. Am. 77, 631–662.

Qiu, X., Priestley, K., McKenzie, D., 1996. Average lithospheric structure of southern Africa. Geophys. J. Int. 127, 563–587.

Randall, D.E., 1989. Efficient calculation of differential seismograms for lithospheric receiver functions. Geophys. J. Int. 99, 469–481.

Reeves, C.V., Hutchings, D.C., 1975. Crustal structure in central southern Africa. Nature 254, 408–410.

Sandvol, E., Seber, D., Calvert, A., Barazangi, M., 1998. Grid search modelling of receiver functions: Implications for crustal structure in the Middle East and North Africa. J. Geophys. Res. 103, 26899–26917.

Shaw, P., Orcutt, J., 1985. Waveform inversion of seismic refraction data and applications to young Pacific crust. Geophys. J. R. Astron. Soc. 82, 375–414.

Stuart, G.W., Zengeni, T.G., 1987. Seismic crustal structure of the Limpopo mobile belt, Zimbabwe. Tectonophysics 144, 323–335.

Vail, R.J., 1967. The southern extension of the east African rift system and related igneous activity. Geol. Rundsch. 57, 601–614.

Van Zijl, J.S.V., 1978. The relationship between the deep electrical resistivity structure and tectonic provinces in southern Africa. Part 1. Results obtained by Schlumberger soundings. Trans. Geol. Soc. S. Afr. 81, 129–142.

Vinnik, L.P., Green, R.W.E., Nicolaysen, L.O., Kosarev, G.L., Petersen, N.V., 1996. Deep seismic structure of the Kaapvaal craton. Tectonophysics 262, 67–75.

Willmore, P.L., Hales, A.L., Gane, P.G., 1952. A seismic investigation of crustal structure in the western Transvaal. Bull. Seismol. Soc. Am. 42, 53–80.

Wright, J.A., Hall, J., 1990. Deep seismic profiling in the Nosop Basin, Botswana: cratons, mobile belts and sedimentary basins. Tectonophysics 173, 333–343.